



CHORUS

This is the accepted manuscript made available via CHORUS. The article has been published as:

Triaxiality in the mid-shell nucleus ${}^{112}\text{Pd}$

A. Esmaylzadeh, V. Karayonchev, G. Häfner, J. Jolie, M. Beckers, A. Blazhev, A. Dewald, C. Fransen, A. Goldkuhle, L. Knafla, and C. Müller-Gatermann

Phys. Rev. C **103**, 054324 — Published 25 May 2021

DOI: [10.1103/PhysRevC.103.054324](https://doi.org/10.1103/PhysRevC.103.054324)

Study of triaxiality in the mid-shell nucleus ^{112}Pd

A. Esmaylzadeh,^{1, a} V. Karayonchev,¹ G. Häfner,^{1,2} J. Jolie,¹ M. Beckers,¹ A. Blazhev,¹
A. Dewald,¹ C. Fransen,¹ A. Goldkuhle,¹ L. Knafla,¹ and C. Müller-Gatermann^{1,3}

¹Universität zu Köln, Mathematisch-Naturwissenschaftliche Fakultät, Institut für Kernphysik, D-50937 Köln, Germany

²Univeristé Paris-Saclay, IJCLab, CNRS/IN2P3, F-91405 Orsay, France

³Argonne National Laboratory, 9700 South Cass Ave, Argonne, IL 60439, United States

(Dated: April 30, 2021)

Lifetimes of low-spin excited states in ^{112}Pd were measured using the recoil-distance Doppler-shift technique. The nucleus of interest was populated in a $^{110}\text{Pd}(^{18}\text{O},^{16}\text{O})^{112}\text{Pd}$ reaction using the Cologne FN Tandem accelerator. Three lifetimes of ground-state band members and one lifetime of the γ band were measured. From these lifetimes reduced transition probabilities were extracted and compared to interacting boson model, γ -soft calculations and Davydov calculations. The lifetime of the 2_2^+ gives some insights on the nuclear shape and structure of the γ band. The deduced transition rates show an indicator for a rigid triaxial nucleus as well as more indicators for a γ -soft nucleus.

I. INTRODUCTION

The isotopic chains of molybdenum, ruthenium and palladium show evidence of γ -soft and rigid triaxial rotor behavior [1–5]. In even-even nuclei, the γ -band is usually based on a 2^+ state that is strongly related to triaxial motions, whereas the 2_1^+ state is primarily sensitive to the quadrupole deformation [6]. The γ band head energy is related to the softness of vibrational motion in the γ direction and the $E_{2_2^+}/E_{4_1^+}$ ratio and the $E_{2_2^+}/E_{2_1^+}$ ratio are important signatures of triaxiality. A triaxial shape rotates around all three axes of the intrinsic body and has its potential energy surface minimum between $\gamma = 0^\circ$ (prolate) and $\gamma = 60^\circ$ (oblate). Two models which discuss the γ unstable case and the triaxial shape are the Wilets-Jean γ -unstable rotor model [7] and the Davydov-Filipov rigid triaxial rotor model [8–10], respectively. The former has a γ -independent minimum in the potential energy surface for a given deformation parameter β where the 2_2^+ and 4_1^+ states are degenerated, while the latter predicts that the 2_2^+ state lies below the 4_1^+ at the maximum of triaxiality at $\gamma = 30^\circ$. To distinguish between the γ softness and rigidity of a nucleus, the energy spacing within the γ band is a good indicator [11]. The staggering parameter $S(J)$ is able to characterize the rigidity or softness of a nucleus and is defined as [11]:

$$S(J) = \frac{[E(J) - 2E(J-1) + E(J-2)]}{E(2_1^+)}. \quad (1)$$

In this case, $E(J)$ represents the energy of the level with spin J in the γ band. If the staggering parameter $S(J)$ is positive for odd-spin levels and negative for even-spin levels, a γ -unstable nucleus is assumed, whereas the γ -rigid case is described by the opposite case [12].

The lower mass Pd isotopes $^{108,110}\text{Pd}$ show indicators of vibrational behavior and the staggering parameter indicates evidence of a γ -soft rotor [20, 21]. Figure 1 shows the staggering parameter for the $^{108-116}\text{Pd}$ isotopes ($Z = 46$). Below $N = 66$ (^{112}Pd), the nuclei exhibit a γ -soft pattern, where the

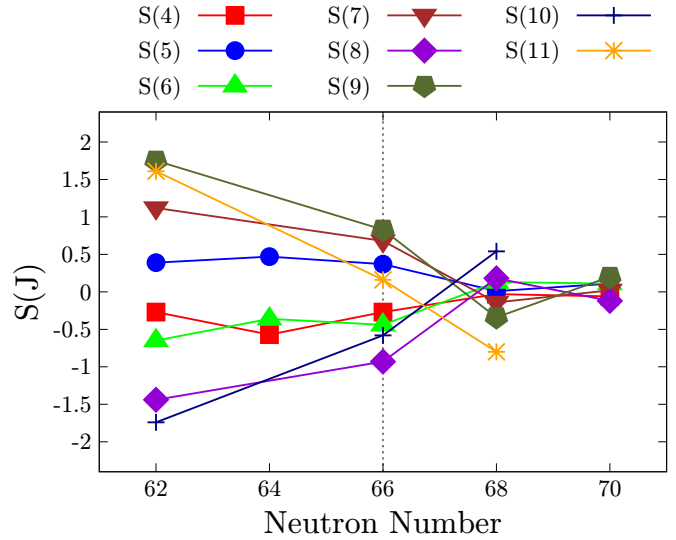


Figure 1. The staggering parameter $S(J)$ for the $^{108-116}\text{Pd}$ isotopes calculated using Eq. (1), where ^{112}Pd is indicated with the dashed line at $N = 66$ (adapted from Ref. [13]). The energy values are taken from ^{108}Pd ($N = 62$) [14], ^{110}Pd ($N = 64$) [15], ^{112}Pd ($N = 66$) [16, 17], ^{114}Pd ($N = 68$) [16, 18] and ^{116}Pd ($N = 70$) [16, 19]. Note that some energy levels are in parenthesis, which means that the spins are not finally assign. This holds especially for the states with spin higher than $J=7$.

staggering parameter $S(J)$ for even spins J are lower compared to the odd J cases. As the chain is approaching $N = 68$ (^{114}Pd), the staggering parameter for the higher spin states ($J > 5$) follow the behavior expected for a triaxial rotor [22]. The investigations of higher mass $^{116-120}\text{Pd}$ ($N = 70 - 74$) isotopes suggest an anharmonic vibrator with less collectivity [16, 23, 24].

^{112}Pd ($N = 66$) lies at the neutron mid shell between $N = 50$ and $N = 82$. A rotational collectivity is expected that has its maximum at $N = 68$ (^{114}Pd) for the isotopic chain [25]. The $R_{4/2} = E(4_1^+)/E(2_1^+)$ ratio increases from 2.4 (^{104}Pd) up to a maximum of 2.6 (^{114}Pd) and afterwards starts to decrease down to 2.4 in ^{120}Pd . The $B_{4/2} = B(E2; 4_1^+ \rightarrow 2_1^+)/B(E2; 2_1^+ \rightarrow 0_1^+)$ ratio is an additional signature which is usually used to char-

^a Corresponding author: aesmaylzadeh@ikp.uni-koeln.de

acterize the shape and behavior of a nucleus. The ratio has already been studied in different works. Starting with $^{108,110}\text{Pd}$ where the ratio is around ≈ 1.5 [20, 26–33], going to the recent lifetime measurements of ^{114}Pd where a ratio of 0.8 has been determined [13]. Furthermore, the nucleus ^{114}Pd was proposed to be an even-even wobblers [16], a phenomenon that has been observed in its isotone ^{112}Ru [34]. The neighboring ruthenium ($Z = 44$) isotopes show γ -soft and rigid triaxial behavior, especially well pronounced for $^{110,112}\text{Ru}$ where the maximum of triaxiality is reached [1, 2, 35, 36]. The former is the corresponding isotone of ^{112}Pd , where a similar behavior could be expected. The ground-state band of the cadmium isotopes $^{108-114}\text{Cd}$ were described as quadrupole vibrational states, but a recent study showed evidence of multi-shape coexistence in $^{110,112}\text{Cd}$, where the ground state shows a distinct minimum at an axial prolate deformation $\beta \approx 0.15$ [37, 38]. To increase the insights of this diverse region of the nuclear chart, the nucleus ^{112}Pd has been investigated in this work. Lifetimes of four low-spin states have been measured and the deduced transition probabilities are discussed in the context of the interacting boson model (IBM), a modified Willets-Jean model and the Davydov-Filipov model to investigate the nuclear shapes and behavior in this region.

II. EXPERIMENT

The nucleus of interest was populated using a two-neutron transfer reaction, i.e. $^{110}\text{Pd}(^{18}\text{O}, ^{16}\text{O})^{112}\text{Pd}$. An average beam current of ~ 1 pnA with an energy of 56 MeV was provided by the Cologne 10 MV FN-Tandem accelerator. The highly enriched (99.98%) ^{110}Pd self-supporting target with a thickness of 0.7 mg/cm 2 was stretched inside the Cologne Plunger device [39]. A 6.5 mg/cm 2 Ta stopper foil was stretched in parallel to the target and acts as a stopper for the ejectiles. To detect the γ rays produced in the reaction, eleven high-purity germanium (HPGe) detectors were mounted in two rings (backward and forward) around the target chamber. The six forward detectors were positioned at an angle of 45° , whereas the five backward detectors were placed at an angle of 142° with respect to the beam direction. Similar to a previous experiment using the same configuration [40], six solar cells were installed at backward angles to detect the light backscattered recoiling fragments. To apply the recoil distance Doppler-shift (RDDS) technique, eleven target-to-stopper distances (40, 59, 89, 109, 139, 239, 339, 489, 639, 789, 1039 μm) have been measured in 90h of beam time. These distances were obtained by using the capacitance method which is described in Ref. [39, 41]. The velocity of the recoiling ^{112}Pd was determined using the shifted and unshifted components of the most intensive transitions and results in $v/c = 1.81(1)\%$. The sum of all particle-gated γ -ray spectra of each distance is shown in Fig. 2. A partial level scheme of ^{112}Pd is shown, where the dashed lines describe possible feeding transitions. Additionally, the 737 keV transition of the 2_2^+ and its low intensity. The strongest γ rays belong to ^{110}Pd , ^{112}Pd and ^{181}Ta . The exclusion of the Coulomb excitations of ^{110}Pd was not possible because due to the low energy

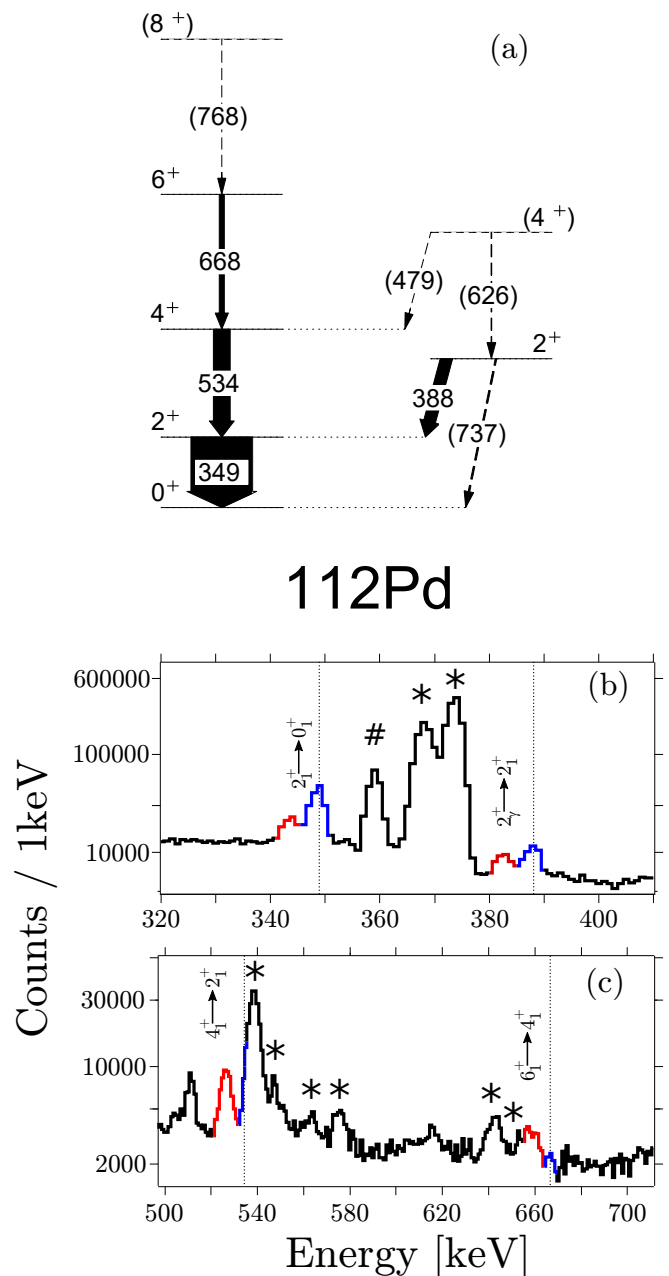


Figure 2. (Color online) (a) The level scheme of the observed states in ^{112}Pd , where the width of the transition arrows indicates the intensity (see Tab. I). Dashed lines have been used to indicate possible feeding transitions, which have not been observed in this experiment. (b)+(c) The γ -ray spectrum with the sum over all distances using a particle gate on the backscattered $^{16,18}\text{O}$ fragments for the backward detectors are shown. All transitions which have been observed in the current work have been colored blue for the unshifted and red for the shifted components. Additionally, a dashed line is indicating the unshifted peak. The transitions marked with a # belong to ^{181}Ta which was the stopper and transitions marked with a * belong to the Coulomb excitation channel, i.e. ^{110}Pd . Note the logarithmic y-scale due to statistical reasons.

Table I. Relative transition intensities observed in the two neutron transfer $^{110}\text{Pd}(^{18}\text{O},^{16}\text{O})^{112}\text{Pd}$ reaction. The intensities were normalized to the $2_1^+ \rightarrow 0_1^+$ transition and the energies are taken from ref [17].

Transition	Transition energy [keV]	Intensity
$2_1^+ \rightarrow 0_1^+$	348.6	1000(19)
$2_\gamma^+ \rightarrow 2_1^+$	388.0	196(21)
$4_1^+ \rightarrow 2_1^+$	534.3	277(20)
$6_1^+ \rightarrow 4_1^+$	667.5	83(26)

resolution the solar cells were not able to separate the recoiling ^{16}O and ^{18}O particles in the spectrum. Hence, the major peaks in the spectrum belong to the Coulomb excitation of the target (^{110}Pd). Furthermore, γ rays from the stopper (^{181}Ta) are visible where the beam particles can scatter and enter the solar cells. The peaks of the backscattered ^{18}O or ^{16}O particles from the target or stopper overlap in the solar cell spectrum and a complete separation of the γ rays from ^{181}Ta was not possible. Some transitions of ^{111}Pd and ^{124}Xe were detected, which were populated in the single neutron transfer and in the fusion evaporation reaction, respectively. The transitions belonging to ^{112}Pd with their energies and intensities, normalized to the $2_1^+ \rightarrow 0_1^+$ transition, are summarized in Table I. During the analysis process, the intensities are used to determine the feeding population for the different states of interest.

III. ANALYSIS

To determine the lifetimes of the 2_γ^+ , 6_1^+ , 4_1^+ and 2_1^+ states, the Bateman equations were used to analyze the recoil distance Doppler-shift data. In addition, the well established differential decay curve method (DDCM) [42] has been used, which is able to detect certain systematic errors. Due to the low statistics of the experiment, only particle-gated γ spectra were used to analyze the data. For a detailed review of both methods, the reader is referred to Ref. [39].

Due to the low statistics for the 6_1^+ state, the method explained in Ref. [43] is used to obtain the lifetimes from the summed spectra of all distances. Here the solution of the Bateman equations of the single distances j is given by:

$$R_{sum} = \frac{\sum_j I_j^u}{\sum_j I_j^u + \sum_j I_j^s} = \sum_j n_j R(t_j) \quad (2)$$

where I_j^u and I_j^s are the intensities of the unshifted and shifted component, respectively. In Eq. (2), n_j describes the normalization factor for each distance, whereas t_j describes the flight-time for each distance. The lifetime of the 6_1^+ state is important to adjust the feeding pattern for the lower-lying states, i.e. the 2_γ^+ and the 4_1^+ state. Hence, a top-to-bottom approach was used to determine the lifetimes.

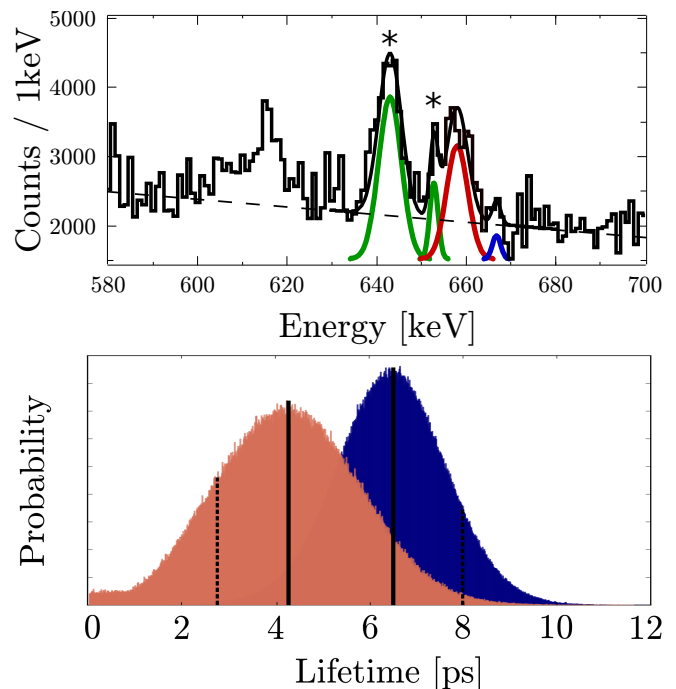


Figure 3. (Color online) (a) Fit of the decaying γ ray of the 6_1^+ state with the unshifted peak at 667.5 keV and the corresponding shifted peak at 658 keV, where the summed particle gated γ -ray spectrum of each distance were used due to the low statistics. The ratio R_{sum} was obtained with a fit and was used to determine the lifetime according to Eq. 2. The peaks marked with an asterisk are the shifted and unshifted component of the $6_1^+ \rightarrow 4_1^+$ transition in ^{110}Pd . A fit to those components (green) has been included to eliminate the contributions on the investigated case where the shifted component is colored in red and the unshifted in blue. (b) The simulated lifetimes of the 6_1^+ state with (red) and without (blue) feeding. See text for details of the simulation. The upper and lower limits of the results are indicated with dashed lines.

A. The analysis of the 6_1^+ state

For the 6_1^+ state as the highest observed state, the spectra for each distance have been summed up to obtain enough statistics. The particle-gated γ -ray spectrum of the backward ring for this state is shown in Fig. 3. The value R_{sum} is obtained using Eq. (2). To extract the lifetime, it is very important to determine the normalization factors carefully. Therefore, a gate on both components of the $2_1^+ \rightarrow 0_1^+$ have been applied. The resulting particle spectrum have been integrated to obtain the normalization factors. The final lifetime is calculated by a Monte-Carlo simulation (with 10^6 iterations), where different parameters are varied. The parameters R_{sum} , normalization factors n_j and the velocity are varied within their uncertainties. Furthermore, the target-to-stopper distance was varied by $\pm 5\mu\text{m}$ and the uncertainties are again obtained using a Monte-Carlo simulation. In Fig. 3(b), the final result is shown where a lifetime of $\tau_{6_1^+} = 6.4(11)\text{ps}$ is obtained for the 6_1^+ state without considering feeding. In a two neutron transfer experiments using the (t,p) reaction, the 8_1^+ state was observed, which is not observed in this experiment [44]. To investigate

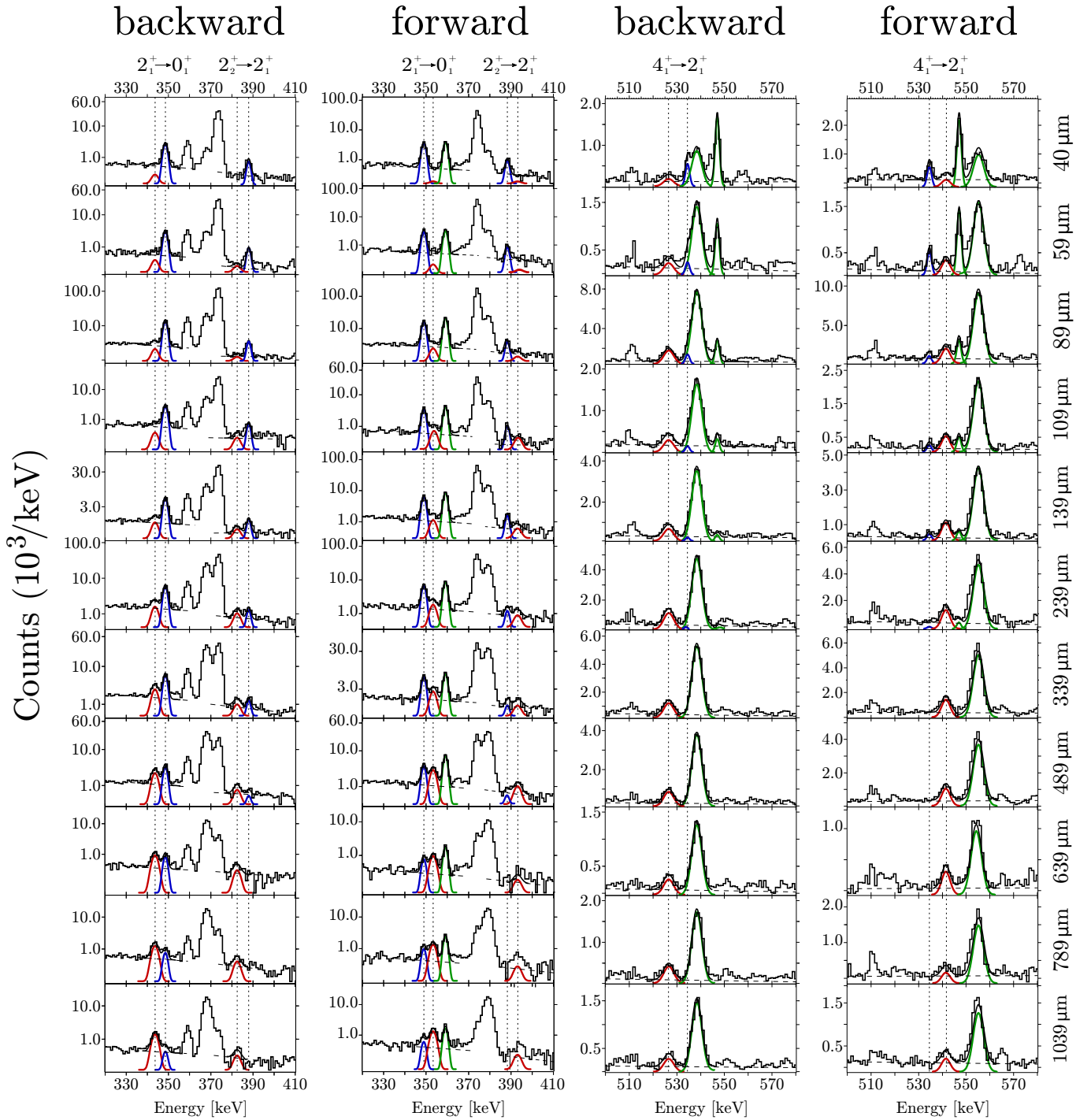


Figure 4. (Color online) Particle-gated spectrum of the backward and forward ring for all distances and the evolution of the $2_1^+ \rightarrow 0_1^+$ (348.6 keV), $2_2^+ \rightarrow 2_1^+$ (388.0 keV) and $4_1^+ \rightarrow 2_1^+$ (534.3 keV) transitions. The ring and the transition are indicated on the upper part of the figure. Furthermore, the distance is placed on the right hand side of the figure. The spectra indicate the background level, the shifted peak (red), the unshifted peak (blue) and also different disturbing transitions which were also fit (green). The disturbing transitions belong either to ^{110}Pd or to ^{181}Ta . Note that a logarithmic scale is used for the backward and forward spectra for the region 320 keV up to 410 keV.

the possible feeding of the 8_1^+ and other unobserved feeding γ rays, the simulation is extended with an extra parameter which considers this feeding. An assumption for maximal feeding from the 8_1^+ state and the unobserved one can be extrapolated

from the feeding of the lower-lying states and by the fact that the population of states in transfer reaction is decreasing with increasing spin and excitation energies. According to the relative intensities given in Tab. I, a realistic amount of the 6_1^+

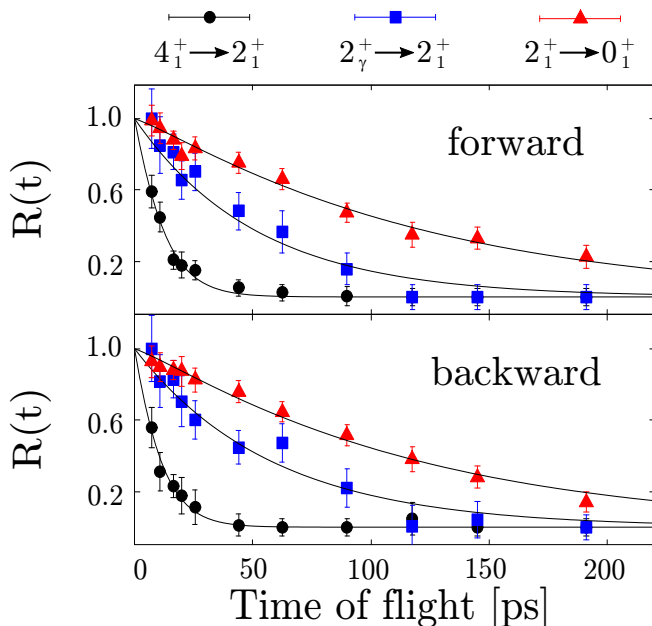


Figure 5. (Color online) The decay curves for the lifetime of the 4_1^+ , 2_2^+ and 2_1^+ states using the Bateman equations to fit the data. The upper panel shows the data points of the forward ring at 45° and the lower panel of the backward ring at 142° . The resulting lifetimes are summarized in Tab. II.

state feeding contribution is 10%. In other words, 90% of the observed 6_1^+ state is directly populated through the reaction. The effective lifetime of the feeding states was chosen to be 100 ps, which is sufficiently long so that the feeding effect is reaching saturation. For the sake of simplicity, the feeding is modeled by a single hypothetical state. By including feeding in the simulation, the calculated lifetime becomes lower and results in $\tau_{6_1^+} = 4.2(15)$ ps (see Fig. 3(b)), where the lower limit (of the simulation with the inclusion of feeding) is used as a lower limit for the lifetime. The final result of the lifetime is $\tau_{6_1^+} = 6.4_{-3.7}^{+1.1}$ ps. The lifetime of the 6_1^+ state in combination with the determined relative intensities can be used to correct feeding contributions to lower states.

B. The lifetime of the 4_1^+ , 2_2^+ and 2_1^+ states

After obtaining the lifetime of the highest observed state the lifetime of the lower-lying states can be determined starting with the 4_1^+ state. The lifetime and feeding population of the 6_1^+ state and the direct population of the 4_1^+ state are used as fixed parameters whereas the lifetime of the 4_1^+ state is the only free parameter to fit the data using the Bateman equations. The evolution of the shifted and unshifted peaks is shown in the third and fourth column of Fig. 4 and the decay curve using the Bateman equations is shown in Fig. 5. Furthermore, in Fig. 6 the results of the backward ring using the DDCM are shown, where the program NAPATAU [45] was used to determine the lifetime. The results for the DDCM and Bateman equations for the backward and forward ring are summarized in Tab. II

Table II. Lifetimes measured in the experiment using the Bateman equation (BE), the DDCM method together with the adopted values. The results from Ref. [46] are given for comparison.

State	Lifetime [ps]					
	Backward ring		Forward ring		Adopted	Lit.
2_1^+	105(9)	112(5)	108(10)	110(5)	110(3)	121(20) ^a
2_2^+	57(7)	51(4)	56(7)	48(4)	51.2(25)	—
4_1^+	8.9(18)	9.2(16)	10.3(15)	11.2(14)	10(1)	—
6_1^+	$6.4_{-3.7}^{+1.1}$	—	—	—	$6.4_{-3.7}^{+1.1}$	—

^a From Ref. [46]

in which the final result of $\tau_{4_1^+} = 10(1)$ ps was obtained.

For the lifetime determination of the 2_2^+ state, the 388 keV $2_2^+ \rightarrow 2_1^+$ transition was used. The 737 keV transition cannot be used because the intensity was too small to extract the lifetime information from the data. The corresponding fit of the data is shown in the first and second column of Fig. 4. The high statistical error is based on the low population of the 2_2^+ state and the disturbing 373 keV transition from ^{110}Pd . After applying the Bateman equations and the DDCM, the final result is $\tau_{2_2^+} = 51.2(25)$ ps, which is the weighted average of four determined lifetimes (see Tab. II).

After obtaining the lifetimes of all states above the 2_1^+ state, the lifetime of this state is now accessible and the feeding pattern can be included in its calculation. The 2_1^+ state is fed by the 2_2^+ state (388 keV) and the 4_1^+ state (534 keV). The fit of the shifted and unshifted peaks are shown in Fig. 4. For the forward angles, the 359 keV transition from ^{181}Ta was included in the fit to take care of the background influence on the shifted $2_1^+ \rightarrow 0_1^+$ (349 keV) transition with the energy 353 keV. After using the Bateman equations and the DDCM, that is shown in Figs. 5 and 6, a final lifetime for the 2_1^+ state of $\tau_{2_1^+} = 110(3)$ ps is obtained. The determined lifetime is consistent with a former RDDS lifetime measurement with a result of 121(20) ps [46] within the errors. Another upper limit of $\tau < 1$ ns can be confirmed as well [47].

IV. THEORETICAL CALCULATIONS

Three phenomenological models were used to describe the excited states and transition rates of ^{112}Pd , namely the Davydov-Filipov [8, 9] and a modified version of the Wilets-Jean model described in Ref. [7, 48, 49] and the sd-interacting boson model (IBM-1). The Davydov-Filipov model represents a general phenomenological approach for quadrupole deformations where the nuclear deformation β and asymmetry parameter γ are fixed parameters for a given $\gamma \neq 0$. In this work, two calculations using $\gamma = 27.5^\circ$ and $\gamma = 30^\circ$ have been used to compare with the experimental signatures. For further details of the model the reader is referred to Refs. [8, 9]. The

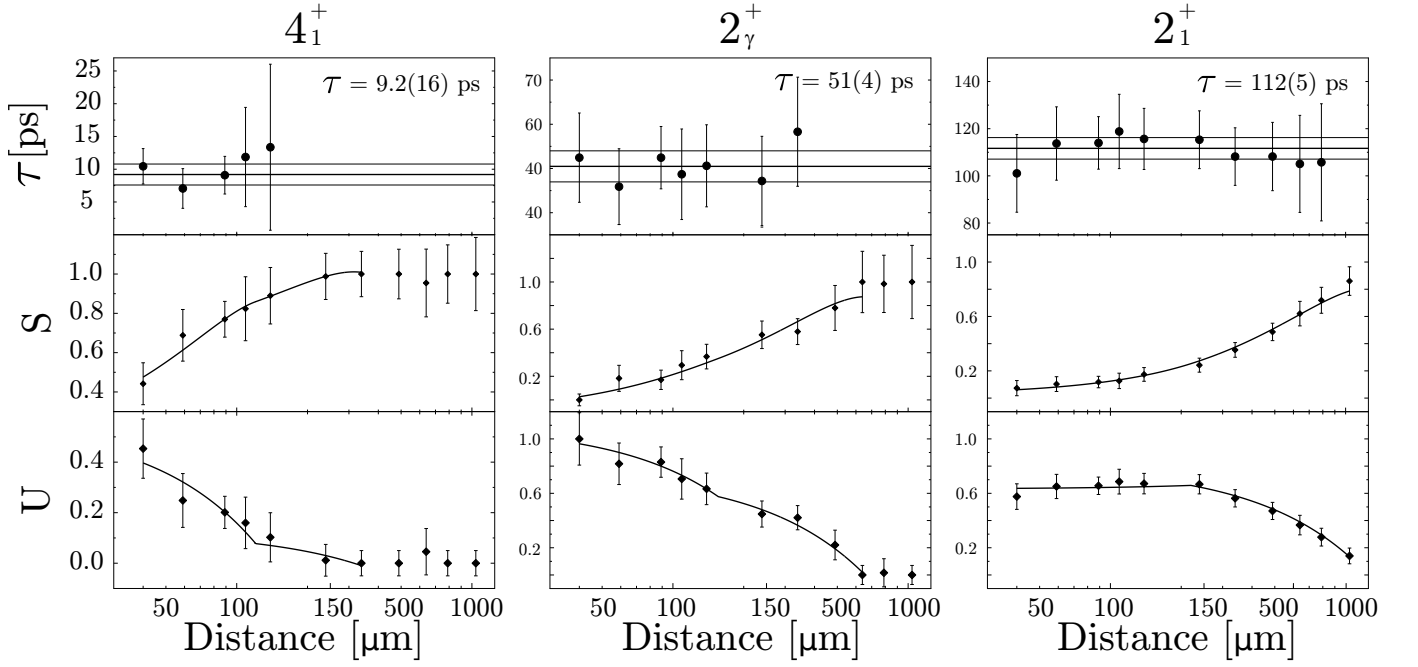


Figure 6. The DDCM method for the 4_1^+ , 2_2^+ and 2_1^+ using the program NAPATAU [45] for the backward angle. The upper panel shows the individually obtained lifetime. The middle panel shows the evolution of the shifted component and the fit which is used to obtain the derivative $\frac{d}{dx}R_i(x)$. Whereas, the unshifted component and the corresponding fit is shown in the lower panel.

second phenomenological approach is a generalization of the Willets-Jean model [7], where the Hamiltonian has a γ independent potential and a constant mass parameter. In addition, the model describes a smooth transition from the standard quadrupole vibrational model through to large β deformation. Here, the reader is referred to Refs. [48, 49] to get further details of the calculations and to Ref. [50] where the code used to calculate the excitation energies and transition probabilities are presented. Additional calculations were performed in the framework of the IBM-1, where no distinction between protons and neutrons is made. This model cannot yield triaxial deformation [51], but only either γ -soft deformation (γ independent), prolate ($\gamma = 0^\circ$) or oblate ($\gamma = 60^\circ$) deformation. In the following, the IBM-1 Hamiltonian and the transition-rate operators are described.

A. Framework of the IBM-1

For the sd IBM-1 calculations, the extended consistent Q formalism (ECQF) [52] with a Hamiltonian similar to the one in Ref. [53]:

$$\hat{H} = \epsilon_d \hat{n}_d + \kappa \hat{Q}^\chi \cdot \hat{Q}^\chi + \lambda \hat{L} \cdot \hat{L} + c_3 \hat{T}_3 \cdot \hat{T}_3, \quad (3)$$

where

$$\begin{aligned} \hat{Q}^\chi &= (s^\dagger \tilde{d} + d^\dagger \tilde{s})^{(2)} + \chi (d^\dagger \tilde{d})^{(2)}, \\ \hat{L} \hat{L} &= \sqrt{10} (d^\dagger \tilde{d})^{(1)}, \\ \hat{T}_3 &= (d^\dagger \tilde{d})^{(3)}, \end{aligned}$$

and $\hat{n}_d = d^\dagger \cdot \tilde{d}$ is used. The E2 operator is defined as:

$$\hat{T}(E2) = e_B \hat{Q}, \quad (4)$$

where e_B is the effective boson charge. The Hamiltonian of Eq. (3) uses five parameters, namely ϵ , κ , λ , c_3 and χ and the code ARBMODEL [54] has been used to perform the calculations. Having four proton holes to the closed proton shell at $Z = 50$ and 16 neutron holes (particles) to the closed neutron shell at $N = 50$ (or $N = 82$) the boson number for ^{112}Pd is $N_B = 10$. In general, some key observables are taken into account to obtain the parameters [55]. The parameters are deduced by a fit to the following ratios:

- $R_{4/2} = E(4_1^+)/E(2_1^+) = 2.53$
- $R_{6/2} = E(6_1^+)/E(2_1^+) = 4.45$
- $R_{2_\gamma/2} = E(2_\gamma^+)/E(2_1^+) = 2.11$
- $B_{4/2} = B(E2; 4_1^+ \rightarrow 2_1^+)/B(E2; 2_1^+ \rightarrow 0_1^+) = 1.29$

A full parameter scan of the five parameters (ϵ , λ , κ , c_3 , χ) in combination with a least χ^2 -fit to the experimental ratios was used to determine the optimal parameters. The parameters $\epsilon = 1124$ keV, $\lambda = 0$ keV, $\kappa = -42$ keV, $c_3 = -179$ keV and $\chi = -0.183$ yield the best agreement to the experimental data. The c_3 term needed to adjust the γ band energy levels to the observed excitation energies. The effective boson charge in the units of eb was chosen to be $e_B = 0.0847$ in order to match the experimental $B(E2; 2_1^+ \rightarrow 0_1^+)$ value. For ^{112}Pd the level energies of the yrast-band up to the 10_1^+ state and for the γ band up to the 6_γ^+ state have been determined. In addition, reduced

transition probabilities have been calculated for the transitions determined in this work.

V. RESULTS AND DISCUSSION

A. Comparison to calculations

1. Energy levels

The energy levels of the experimental data and the calculations, namely IBM-1, γ -soft and the Davydov-Filipov (hereafter D-F) calculations, are shown in Fig. 7. Starting with the ground state band and the 2_1^+ state, where all models are able to describe the excitation energies. The ground state band members 4_1^+ and 6_1^+ are well described by the IBM-1 while both D-F calculations overestimate the energy by around 50 keV and around 200 keV. Due to the properties of the γ -soft model, the energy of the 4_1^+ and 2_2^+ are described as a doublet and the 3_2^+ , 4_2^+ and 6_1^+ states as a triplet state. The energy of the 4_1^+ state is underestimated as well as the energy of the 6_1^+ . The only model that is able to describe the 8_1^+ and 10_1^+ states with relatively good accuracy is the IBM-1. The D-F calculation is overestimating the excitation energy of those states while the γ -soft model underestimates the excitation energy, both by about 500 keV. The γ bandhead, the 2_2^+ state is well described by the IBM-1 calculation and the D-F calculations with 27.5° , whereas the doublet state in the γ -soft overestimates the excitation energy. The IBM-1 is the only model that is able to describe the other γ -band members while slightly underestimating the excitation energy. The energy level of the γ band using the γ -independent potential (γ -soft model) cluster as (2_γ^+) , $(3_\gamma^+, 4_\gamma^+)$ and $(5_\gamma^+, 6_\gamma^+)$ whereas the rigid triaxial rotor (Davydov-Filipov model) show a $(2_\gamma^+, 3_\gamma^+)$, $(4_\gamma^+, 5_\gamma^+)$ clustering pattern [56]. The experimental level energies do not favor either of the γ -soft and D-F models and, hence, neither of the models describe the energy pattern. An argument which could support that the γ -soft-type cluster pattern is slightly favored is due to the energies of the 3_γ^+ and the 5_γ^+ states which are closer to the 4_γ^+ and 6_γ^+ states, respectively. A further signature is the staggering parameter that can be calculated using Eq. (1) and is shown in Fig. 8 for the experimental data and compared to the calculations. Note that the staggering values of the $S(8)$ is also shown whereas the level energies of the corresponding 8_γ^+ states is not shown in Fig. 7 for the D-F calculations. The experimental $S(J)$ values of ^{112}Pd occur to have small oscillations around zero where the even $S(J)$ values are negative and the odd $S(J)$ values positive. This behavior suggests a γ -soft pattern, where the γ -soft calculations are reproducing the pattern but are noticeably higher. Due to the rigid properties of the D-F calculations, an opposite behavior is observed and, hence, both are not able to describe the experimental oscillation of the $S(J)$ values. As for the energy levels, the only model that describes the staggering parameter with good accuracy, are the calculations performed using the IBM-1 model. Comparing the four calculations from the energetically point of view, the IBM-1 is the closest to the experimental observed one. Therefore, a potential energy surface (PES) using the pa-

rameters of the IBM-1 has been used to get a better overview of the β and γ deformation of this nucleus. The potential which is dependent on β and γ is deduced by calculating the expectation value of the Hamiltonian in the coherent state [57–59] and it is shown in Fig. 9. The PES shows a minimum around $\beta \approx 0.3$ and $\gamma = 0^\circ$, which corresponds to prolate deformation. The energy minimum in the PES is broad and spreading in the γ -direction, which could be interpreted as an evidence for γ -softness.

2. Reduced transition probabilities

The reduced transition probabilities are summarized in Tab. III. The calculated $B(E2; 2_1^+ \rightarrow 0_1^+)$ values for the D-F and IBM calculations were normalized to the experimental $B(E2; 2_1^+ \rightarrow 0_1^+)$ value. The γ -soft model was not normalized and therefore the calculations slightly underestimate the value. All calculations obtain an accurate description of the $B(E2; 4_1^+ \rightarrow 2_1^+)$ value, where it is notable that all theoretical predict larger values tht are above the experimentally deduced transition probability. Due to the high uncertainty of the lifetime of the 6_1^+ state, the transition probability ranges from 24 W.u. to 58 W.u. and does not allow for a clear interpretation of the result. All calculations predict $B(E2; 6_1^+ \rightarrow 4_1^+)$ values which are larger. A possible explanation could be a low-lying interband mixing which is not included in the calculations. A further investigation of this state is necessary to get a more accurate $B(E2; 6_1^+ \rightarrow 4_1^+)$ value so that a better description is possible. The $B(E2; 2_2^+ \rightarrow 0_1^+)$ value can only be described by the D-F calculation with $\gamma = 27.5^\circ$. The IBM-1 predicts a larger value and the γ -soft as well as the D-F calculation for $\gamma = 30^\circ$ computed a non existing probability for this transition. The other transition depopulating this state going to the 2_1^+ state is a mixed M1/E2 transition where the multipole mixing ratio of $\delta = 4.7^{+1.7}_{-3.5}$ is taken from Ref. [61]. The relatively large $B(E2; 2_2^+ \rightarrow 2_1^+)$ strength which can be an indicator for a rigid triaxial rotor is reproduced by the IBM-1, whereas the other calculations overestimate the value. Finally, the $B(M1; 2_2^+ \rightarrow 2_1^+)$ is not described by neither calculation because the models are not able to calculation such transitions.

By examining the three ratios $B_{4/2}$, $B_{2_\gamma/2}$, $B'_{2_\gamma/2}$ defined in Tab. III, all models reproduce the $B_{4/2}$ ratio within the three sigma error margin. The $B_{2_\gamma/2}$ ratio compares intraband transition rates where the IBM-1 obtained a similar ratio and the other models can not provide an accurate description of this ratio. The maximal triaxial D-F model with $\gamma = 30^\circ$ and the γ -soft model overestimate the value by a factor of 2, with the same ratio of $B_{2_\gamma/2} = 1.64$. Furthermore, the same overestimation occurs for the $B'_{2_\gamma/2}$ ratio, where both approaches calculated give an infinite value. The D-F calculation at $\gamma = 27.5^\circ$ predicts this ratio with good accuracy whereas the IBM-1 underestimates the ratio.

The following formula:

$$\chi^2 = \sum_i \frac{(x_{\text{theo},i} - x_{\text{exp},i})^2}{\Delta x_{\text{exp},i}} \quad (5)$$

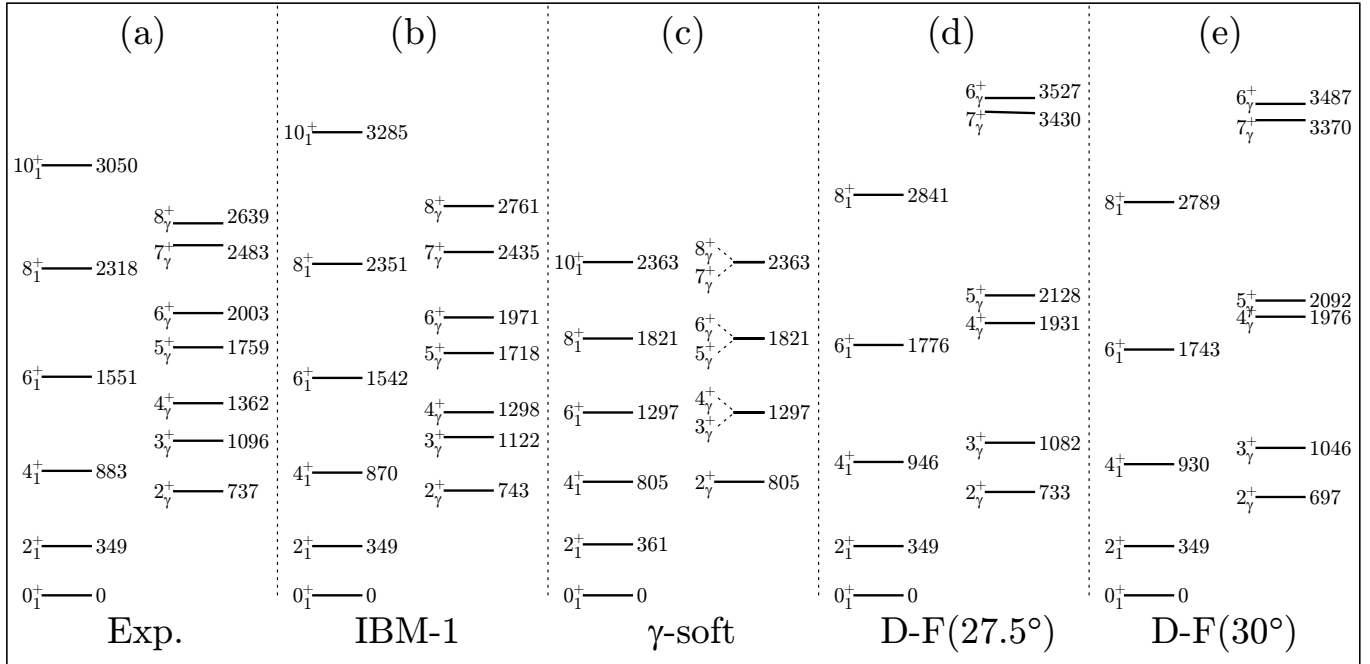


Figure 7. The level energies of the ground state up to the 10_1^+ and the γ -band up to the 8_2^+ state for the (a) experimental (b) the IBM-1 calculations. (c) The γ -soft calculations using the model explained in [48, 49] and using the code from Ref. [50], where the parameters $B = 146$, $a = 0.12$, $C_2 = 47$, $G = 3.42$ and $C_8 = f = 0$ have been used. Lastly, the Davydov-Filippov calculations with (d) $\gamma = 27.5^\circ$ and with (e) $\gamma = 30^\circ$, where the 8_2^+ state is not shown which is positioned at about 5 MeV. All excitation energies are given in keV and a further description of the models and calculations are given in Sec. IV.

Table III. The experimentally deduced transition probabilities for ^{112}Pd compared to the transition rates of the IBM-1, γ -soft and two Davydov-Filippov calculations where one W.u. equals $32.07 e^2 fm^4$. A parameter χ^2 defined in Eq. 5 has been calculated to give a statistical overview of the model with the best description. Three $B(E2)$ ratios are calculated to get a more detailed picture of the comparison.

Transition	Experiment	IBM-1	γ -soft	D-F (27.5°)	D-F (30°)
$B(E2; 2_1^+ \rightarrow 0_1^+)$ [W.u.]	44(1)	44	39	44	44
$B(E2; 4_1^+ \rightarrow 2_1^+)$ [W.u.]	58_{-5}^{+6}	67	64	61	62
$B(E2; 6_1^+ \rightarrow 4_1^+)$ [W.u.]	29_{-5}^{+29}	77	87	77	77
$B(E2; 2_\gamma^+ \rightarrow 0_1^+)$ [W.u.] ^a	0.50(3)	2.1	0	0.7	0
$B(E2; 2_\gamma^+ \rightarrow 2_1^+)$ [W.u.] ^{ab}	40(1)	40	64	55	64
$B(M1; 2_\gamma^+ \rightarrow 2_1^+)$ [$10^{-4} \mu_N^2$] ^{ab}	6.2_{-30}^{+80}	-	-	-	-
χ^2		178	731	307	666
$B_{4/2} = \frac{B(E2; 4_1^+ \rightarrow 2_1^+)}{B(E2; 2_1^+ \rightarrow 0_1^+)}$	1.31(14)	1.52	1.64	1.39	1.41
$B_{2_\gamma/2} = \frac{B(E2; 2_\gamma^+ \rightarrow 2_1^+)}{B(E2; 2_1^+ \rightarrow 0_1^+)}$	0.91(3)	0.91	1.64	1.25	1.64
$B'_{2_\gamma/2} = \frac{B(E2; 2_\gamma^+ \rightarrow 2_1^+)}{B(E2; 2_\gamma^+ \rightarrow 0_1^+)}$	80(5)	19	∞	79	∞

^a A branching ratio of 76% for the $2_\gamma^+ \rightarrow 2_1^+$ and 24% for the $2_\gamma^+ \rightarrow 0_1^+$ has been used [60, 61].

^b A multipole mixing ratio $\delta = -4.7_{-3.5}^{+1.7}$ has been used from Ref. [61].

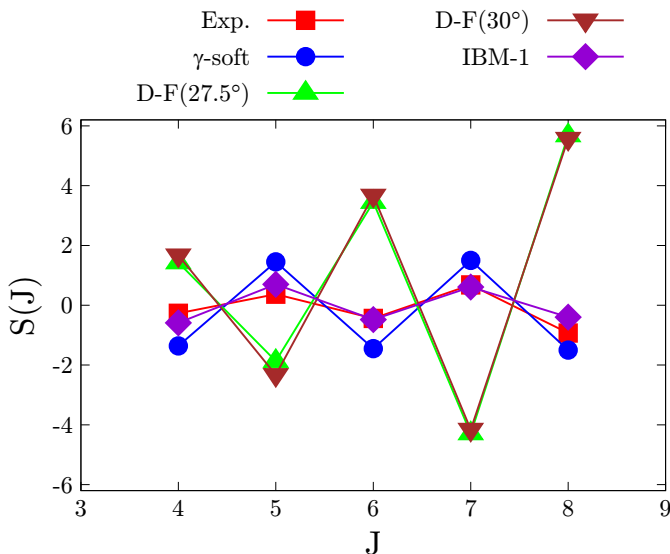


Figure 8. (Color online) The experimentally deduced staggering parameter compare to the staggering parameter of the IBM-1 calculations, γ -soft calculations and the Davydov-Filipov calculations with 27.5° and 30° . For further explanations see text.

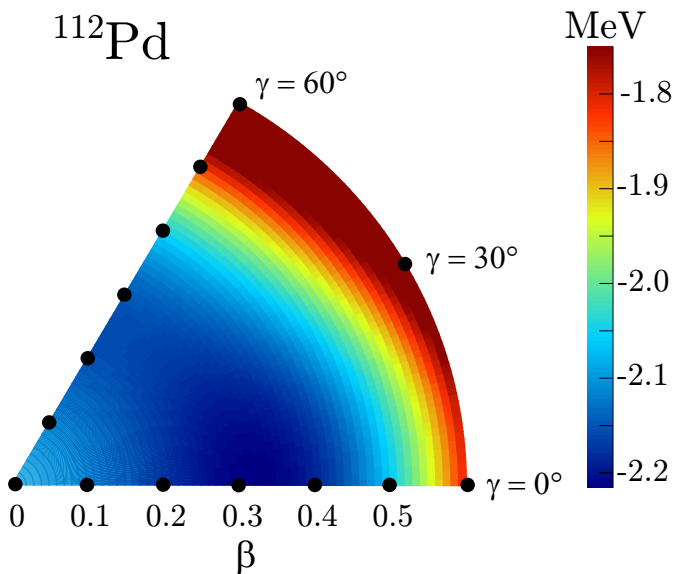


Figure 9. (Color online) The potential energy surface (PES) of the IBM-1 calculation using the parameters described in Sec. IV A.

has been used to statistically describe the model with the most accuracy. The smaller the value the more accurate the calculation. The corresponding values are summarized in Tab. III and the IBM-1 and D-F calculation at $\gamma = 27.5^\circ$ provide the best values.

B. Indicators of triaxiality and γ -softness in ^{112}Pd

With the assumed γ bandhead in combination with the newly reduced transition probabilities $B(E2; 2_2^+ \rightarrow 2_1^+)$ and

$B(E2; 2_2^+ \rightarrow 0_1^+)$ can give insights of the triaxial or γ -soft behavior of this nucleus. Both possible structures are discussed within the newly obtained results in addition to comparisons to isotones and isotopes.

1. Making the case for rigid triaxiality

An indicator of a rigid triaxial rotor nucleus is that the excitation energy of the 2_2^+ state is below the 4_1^+ state. This is the case for the $^{106-118}\text{Pd}$ ($N = 60 - 72$) isotopes. For the isotopic chain of palladium isotopes, the excitation energy of the 2_2^+ has its minimum at ^{114}Pd ($N = 68$) with $E_{2_2^+} = 695$ keV [60]. A similar behavior has been observed for the ruthenium isotopes with a maximum of triaxiality is reached for $^{110,112}\text{Ru}$ [1, 35, 36], where the former is the isotone of ^{112}Pd . This is supported by a recent study of ^{110}Ru where a relative rigid triaxial deformation near the ground state has been suggested [2]. Another experimental relation that supports the rigid triaxiality in this nucleus is that the sum of the energies of the first and second 2^+ states is almost equal to the energy of the 3_1^+ state, i.e. $E(3_1^+) = E(2_1^+) + E(2_2^+)$ [2]. For ^{112}Pd this signature matches with less than 15 keV deviation which indicates a possible breaking of axial symmetry [2]. In addition, the $B(E2)$ reduced transition probabilities between level of a $K = 2$ band, here in this case the γ band, and a $K = 0$ band which is the ground state band are sensitive indicators of triaxial behavior [62]. Due to the relatively large $B(E2; 2_2^+ \rightarrow 2_1^+)$ and small $B(E2; 2_2^+ \rightarrow 0_1^+)$ values, a strong indicator of triaxial deformation is given. This indicators are also supported by the D-F calculations that reproduce the experimental signatures namely the $B(E2; 2_2^+ \rightarrow 0_1^+)$ and $B(E2; 2_2^+ \rightarrow 2_1^+)$ with reasonable accuracy at $\gamma = 27.5^\circ$.

2. Making the case for a γ -soft nucleus

Not all signatures support the fact of a rigid rotor nucleus, some observables favor a γ -soft nucleus. The relatively large $B(E2; 2_2^+ \rightarrow 2_1^+)$ and small $B(E2; 2_2^+ \rightarrow 0_1^+)$ could also be an indicator for γ -softness. Another important characteristic of a γ -soft nucleus is the small increasing $S(J)$ value for increasing spin J (for absolute values), i.e. the $S(4) = -1.36$, $S(5) = 1.45$, $S(6) = -1.45$, $S(7) = 1.50$..., in contrast to the largely increasing $S(J)$ value for increasing spin J (see Fig. 8) in the rigid triaxial case. The experimental staggering parameter increases smoothly with increasing spin J , which is similar to the assumption of a γ -soft nucleus. Another supporting factor is the PES of the IBM-1 which is shown in Fig. 9. Note that these calculation obtained the most accurate description of ^{112}Pd . In Fig. 9, a tendency of γ -softness can be observed as the minimum spreads in the direction of γ . The minimum energy in the PES is not flat in the γ degree of freedom as it is supposed for the γ -soft case and a minimum is visible for a prolate deformation. Observing the neighboring isotopes, ^{110}Pd shows evidences of a γ -soft behavior [21] so that it is reasonable to assume similar behavior for ^{112}Pd with increasing excitation energy. The even-odd nuclei $^{109,111}\text{Pd}$

have been studied in Ref. [63] where an enhanced γ -softness has been observed, which would underline the γ -softness of the Pd-isotopes in this region. Another supporting factor is the overall staggering trend in Mo-Ru-Pd region, which shows a well pronounced staggering effect for $^{108-112}\text{Pd}$ [64]. Note that the staggering amplitudes are strongly suppressed for the isotope ^{110}Ru .

3. Summary

The γ -soft model describes the energetic properties of ^{112}Pd with more accuracy than the rigid triaxial rotor model. On the other hand, the reduced transition probabilities are better described by the D-F calculations, especially for $\gamma = 27.5^\circ$. Both, the γ -soft and rigid triaxial structures have signatures and characteristics that match the experimental data and, hence, a clear conclusion can not be made. A possible hypothesis which could support both models is that the low spin states i.e. 2_γ^+ , 3_γ^+ of the γ band possess a more rigid behavior while the higher spin states $J > 4$ show a γ -soft behavior. This would suggest a smooth transition from a relative rigid nuclear structure in the low spin states to a nearly γ -soft structure in the higher spin states within the γ -band. This hypothesis is supported by the fact that the D-F calculations are capable to describe the lower states of the γ band with better accuracy than the γ -soft calculations and vice versa for the higher spin states. Such a phenomenon lies outside the model space of these models but has been studied for the Ru isotopes via cranked Hartree-Fock-Bogoliubov calculations [65].

The best description is given by the IBM-1. The PES obtained from the IBM calculations show a prolate minimum at $\beta \approx 0.3$ with a broad minimum γ in the degree of freedom which is not but close to γ -soft. To clarify and give a better insight on the shape and structure of ^{112}Pd , lifetime measurements of the 3_γ^+ and 4_γ^+ state would be desirable. With the knowledge of these lifetimes a better description of the nucleus could be reached, especially the reduced transition probabilities using the lifetime of the 4_γ^+ state. An experimental ratio of $B_{4_\gamma/2_\gamma} = B(E2; 4_\gamma^+ \rightarrow 4_1^+)/B(E2; 4_\gamma^+ \rightarrow 2_\gamma^+) \approx 0.95$ can be obtained using the branching ratios given in Refs. [17, 60]. Comparing this experimental signature to the D-F and γ -soft

calculations, a ratio of $B_{4_\gamma/2_\gamma} \approx 0.57$ and $B_{4_\gamma/2_\gamma} \approx 0.91$ can be obtained, respectively. This would be another argument of the mentioned hypothesis and, hence, a further investigation could verify this. An investigation of the γ band transition probabilities in ^{114}Pd would give further experimental signatures to complement the conclusion. Up to now, no experimental transition probabilities within the γ -band in ^{114}Pd are available.

VI. CONCLUSIONS

The lifetimes of the 2_1^+ , 4_1^+ , 6_1^+ and 2_γ^+ states in ^{112}Pd have been measured using the RDDS technique. The results have been compared to IBM-1 calculations, a modified γ -soft calculation and to D-F calculations using two different γ parameters. All four descriptions of the energy levels lead to an overall good description for the lower spin states, whereas the higher spin states are strongly overestimated by all the D-F calculations. The deduced transition probabilities were compared to the models and the IBM-1 calculation reproduces the values with the highest accuracy. The potential energy surface using the IBM-1 parameters does not show a clear minimum at $\gamma = 30^\circ$, which would be the case for a triaxial rotor nucleus, nor a γ -soft behavior. A shallow minimum at $\gamma = 0^\circ$ is shown, which is not completely free in the γ degree of freedom which would support a γ -soft nucleus. Further investigations of lifetimes in the γ band would be of interest to complete the observations of this work.

Acknowledgments

We thank the operator team of the IKP FN Tandem accelerator for the professional support during the experiment. A. E. and V.K. acknowledge the support by the BMBF under Grant No. 05P15PKFNA. The authors also thank Jacek Dobaczewski for providing the code to calculate the energies of the γ -soft and Davydov-Filipov model. G.H. acknowledges support from the Bonn-Cologne Graduate School for Physics and Astronomy (BCGS) and the IDEX API grant. C. M. G. is supported by the U. S. Department of Energy, Office of Nuclear Physics, under contract number DE-AC02-06CH11357.

-
- [1] Y. Luo, S. Zhu, J. Hamilton, J. Rasmussen, A. Ramayya, C. Goodin, K. Li, J. Hwang, D. Almed, S. Frauendorf, V. Dimitrov, J. ye Zhang, X. Che, Z. Jang, I. Stefanescu, A. Gelberg, G. Ter-Akopian, A. Daniel, M. Stoyer, R. Donangelo, J. Cole, and N. Stone, *Physics Letters B* **670**, 307 (2009).
- [2] D. Doherty, J. Allmond, R. Janssens, W. Korten, S. Zhu, M. Zielińska, D. Radford, A. Ayangeakaa, B. Bucher, J. Batchelder, C. Beausang, C. Campbell, M. Carpenter, D. Cline, H. Crawford, H. David, J. Delaroche, C. Dickerson, P. Fallon, A. Galindo-Uribarri, F. Kondev, J. Harker, A. Hayes, M. Hendricks, P. Humby, M. Girod, C. Gross, M. Klinte fjord, K. Kolos, G. Lane, T. Lauritsen, J. Libert, A. Macchiavelli, P. Napiorkowski, E. Padilla-Rodal, R. Pardo, W. Reviol, D. Sarantites, G. Savard, D. Seweryniak, J. Srebrny, R. Varner, R. Vondrasek, A. Wiens, E. Wilson, J. Wood, and C. Wu, *Physics Letters B* **766**, 334 (2017).
- [3] H. Watanabe, K. Yamaguchi, A. Odahara, T. Sumikama, S. Nishimura, K. Yoshinaga, Z. Li, Y. Miyashita, K. Sato, L. Próchniak, H. Baba, J. Berryman, N. Blasi, A. Bracco, F. Camera, J. Chiba, P. Doornenbal, S. Go, T. Hashimoto, S. Hayakawa, C. Hinke, N. Hinohara, E. Ideguchi, T. Isobe, Y. Ito, D. Jenkins, Y. Kawada, N. Kobayashi, Y. Kondo, R. Krücken, S. Kubono, G. Lorusso, T. Nakano, T. Nakatsukasa, M. Kurata-Nishimura, H. Ong, S. Ota, Z. Podolyák, H. Sakurai, H. Scheit, K. Steiger, D. Steppenbeck, K. Sugimoto, K. Tajiri, S. Takano, A. Takashima, T. Teranishi, Y. Wakabayashi, P. Walker, O. Wieland, and H. Yamaguchi, *Physics Letters B* **704**, 270 (2011).

- [4] J. Snyder, W. Reviol, D. Sarantites, A. Afanasjev, R. Janssens, H. Abusara, M. Carpenter, X. Chen, C. Chiara, J. Greene, T. Lauritsen, E. McCutchan, D. Seweryniak, and S. Zhu, *Physics Letters B* **723**, 61 (2013).
- [5] P.-A. Söderström, G. Lorusso, H. Watanabe, S. Nishimura, P. Doornenbal, G. Thiamova, F. Browne, G. Gey, H. S. Jung, T. Sumikama, J. Taprogge, Z. Vajta, J. Wu, Z. Y. Xu, H. Baba, G. Benzoni, K. Y. Chae, F. C. L. Crespi, N. Fukuda, R. Gernhäuser, N. Inabe, T. Isobe, A. Jungclaus, D. Kameda, G. D. Kim, Y.-K. Kim, I. Kojouharov, F. G. Kondev, T. Kubo, N. Kurz, Y. K. Kwon, G. J. Lane, Z. Li, A. Montaner-Pizá, K. Moschner, F. Naqvi, M. Niikura, H. Nishibata, A. Odahara, R. Orlandi, Z. Patel, Z. Podolyák, H. Sakurai, H. Schaffner, G. S. Simpson, K. Steiger, H. Suzuki, H. Takeda, A. Wendt, A. Yagi, and K. Yoshinaga, *Phys. Rev. C* **88**, 024301 (2013).
- [6] R. F. Casten, *Nuclear Structure from a Simple Perspective*.
- [7] L. Wilets and M. Jean, *Phys. Rev.* **102**, 788 (1956).
- [8] A. Davydov and G. Filippov, *Nuclear Physics* **8**, 237 (1958).
- [9] A. Davydov and V. Rostovsky, *Nuclear Physics* **12**, 58 (1959).
- [10] A. Davydov and V. Rostovskii, *Soviet Physics JETP* **36** (1959).
- [11] N. Zamfir and R. Casten, *Physics Letters B* **260**, 265 (1991).
- [12] H. Sobhani, H. Hassanabadi, and W. S. Chung, *Nuclear Physics A* **973**, 33 (2018).
- [13] E. R. Gamba, A. M. Bruce, S. Lalkovski, M. Rudigier, S. Bottoni, M. P. Carpenter, S. Zhu, J. T. Anderson, A. D. Ayangeakaa, T. A. Berry, I. Burrows, M. C. Gallardo, R. J. Carroll, P. Copp, D. M. Cullen, T. Daniel, G. F. Martínez, J. P. Greene, L. A. Gurgi, D. J. Hartley, R. Ilieva, S. Ilieva, F. G. Kondev, T. Kröll, G. J. Lane, T. Lauritsen, I. Lazarus, G. Lotay, C. R. Niță, Z. Podolyák, V. Pucknell, M. Reed, P. H. Regan, J. Rohrer, J. Sethi, D. Seweryniak, C. M. Shand, J. Simpson, M. Smoleń, E. A. Stefanova, V. Vedia, and O. Yordanov, *Phys. Rev. C* **100**, 044309 (2019).
- [14] J. Blachot, *Nuclear Data Sheets* **91**, 135 (2000).
- [15] G. Gürdal and F. Kondev, *Nuclear Data Sheets* **113**, 1315 (2012).
- [16] Y. Luo, J. Rasmussen, J. Hamilton, A. Ramayya, S. Frauendorf, J. Hwang, N. Stone, S. Zhu, N. Brewer, E. Wang, I. Lee, S. Liu, G. TerAkopian, A. Daniel, Y. Oganessian, M. Stoyer, R. Donangelo, W. Ma, J. Cole, Y. Shi, and F. Xu, *Nuclear Physics A* **919**, 67 (2013).
- [17] S. Lalkovski and F. Kondev, *Nuclear Data Sheets* **124**, 157 (2015).
- [18] J. Blachot, *Nuclear Data Sheets* **113**, 515 (2012).
- [19] J. Blachot, *Nuclear Data Sheets* **111**, 717 (2010).
- [20] L. Svensson, C. Fahlander, L. Hasselgren, A. Bäcklin, L. Westerberg, D. Cline, T. Czosnyka, C. Wu, R. Diamond, and H. Kluge, *Nuclear Physics A* **584**, 547 (1995).
- [21] S. Lalkovski, A. Minkova, M.-G. Porquet, A. Bauchet, I. Deloncle, A. Astier, N. Buforn, L. Donadille, O. Dorvaux, B. Gall, R. Lucas, M. Meyer, A. Prevost, N. Redon, N. Schulz, and O. Stezowski, *Eur. Phys. J.* **A18**, 589 (2003).
- [22] S. Frauendorf, *International Journal of Modern Physics E* **24**, 1541001 (2015), <https://doi.org/10.1142/S0218301315410013>.
- [23] M. Stoyer, W. Walters, C. Wu, D. Cline, H. Hua, A. Hayes, R. Teng, R. Clark, P. Fallon, A. Goergen, A. Macchiavelli, K. Vetter, P. Mantica, and B. Tomlin, *Nuclear Physics A* **787**, 455 (2007), proceedings of the Ninth International Conference on Nucleus-Nucleus Collisions.
- [24] X. Q. Zhang, J. H. Hamilton, A. V. Ramayya, S. J. Zhu, J. K. Hwang, C. J. Beyer, J. Kormicki, E. F. Jones, P. M. Gore, B. R. S. Babu, T. N. Ginter, R. Aryaeinejad, K. Butler-Moore, J. D. Cole, M. W. Drigert, J. K. Jewell, E. L. Reber, J. Gilat, I. Y. Lee, J. O. Rasmussen, A. V. Daniel, Y. T. Oganessian, G. M. Ter-Akopian, W. C. Ma, P. G. Varmette, L. A. Bernstein, R. W. Lougheed, K. J. Moody, M. A. Stoyer, R. Donangelo, and J.-Y. Zhang, *Phys. Rev. C* **63**, 027302 (2001).
- [25] A. Dewald, K. Starosta, P. Petkov, M. Hackstein, W. Rother, P. Adrich, A. M. Amthor, T. Baumann, D. Bazin, M. Bowen, A. Chester, A. Dunomes, A. Gade, D. Galaviz, T. Glasmacher, T. Ginter, M. Hausmann, J. Jolie, B. Melon, D. Miller, V. Moeller, R. P. Norris, T. Pissulla, M. Portillo, Y. Shimbara, A. Stolz, C. Vaman, P. Voss, and D. Weisshaar, *Phys. Rev. C* **78**, 051302 (2008).
- [26] R. Robinson, F. McGowan, P. Stelson, W. Milner, and R. Sayer, *Nuclear Physics A* **124**, 553 (1969).
- [27] H. H. Bolotin and D. A. McClure, *Phys. Rev. C* **3**, 797 (1971).
- [28] R. Harper, A. Christy, I. Hall, I. Naqib, and B. Wakefield, *Nuclear Physics A* **162**, 161 (1971).
- [29] D. Eccleshall, B. Hinds, and M. Yates, *Nuclear Physics* **32**, 190 (1962).
- [30] P. H. Stelson and F. K. McGowan, *Phys. Rev.* **110**, 489 (1958).
- [31] J. Wesseling, C. de Jager, J. Van Der Laan, H. De Vries, and M. Harakeh, *Nuclear Physics A* **535**, 285 (1991).
- [32] J. W. Lightbody, S. Penner, S. P. Fivozinsky, P. L. Hallowell, and H. Crannell, *Phys. Rev. C* **14**, 952 (1976).
- [33] B. Kotlinski, D. Cline, A. Bäcklin, and D. Clark, *Nuclear Physics A* **503**, 575 (1989).
- [34] J. Hamilton, S. Zhu, Y. Luo, A. Ramayya, S. Frauendorf, J. Rasmussen, J. Hwang, S. Liu, G. Ter-Akopian, A. Daniel, and Y. Oganessian, *Nuclear Physics A* **834**, 28c (2010).
- [35] P. Möller, R. Bengtsson, B. G. Carlsson, P. Olivius, and T. Ichikawa, *Phys. Rev. Lett.* **97**, 162502 (2006).
- [36] I. Stefanescu, A. Gelberg, J. Jolie, P. Van Isacker, P. von Brentano, Y. Luo, S. Zhu, J. Rasmussen, J. Hamilton, A. Ramayya, and X. Che, *Nuclear Physics A* **789**, 125 (2007).
- [37] P. E. Garrett, T. R. Rodríguez, A. D. Varela, K. L. Green, J. Bangay, A. Finlay, R. A. E. Austin, G. C. Ball, D. S. Bandyopadhyay, V. Bildstein, S. Colosimo, D. S. Cross, G. A. Demand, P. Finlay, A. B. Garnsworthy, G. F. Grinyer, G. Hackman, B. Jigmeddorj, J. Jolie, W. D. Kulp, K. G. Leach, A. C. Morton, J. N. Orce, C. J. Pearson, A. A. Phillips, A. J. Radich, E. T. Rand, M. A. Schumaker, C. E. Svensson, C. Sumithrarachchi, S. Triambak, N. Warr, J. Wong, J. L. Wood, and S. W. Yates, *Phys. Rev. Lett.* **123**, 142502 (2019).
- [38] P. E. Garrett, T. R. Rodríguez, A. Diaz Varela, K. L. Green, J. Bangay, A. Finlay, R. A. E. Austin, G. C. Ball, D. S. Bandyopadhyay, V. Bildstein, S. Colosimo, D. S. Cross, G. A. Demand, P. Finlay, A. B. Garnsworthy, G. F. Grinyer, G. Hackman, B. Jigmeddorj, J. Jolie, W. D. Kulp, K. G. Leach, A. C. Morton, J. N. Orce, C. J. Pearson, A. A. Phillips, A. J. Radich, E. T. Rand, M. A. Schumaker, C. E. Svensson, C. Sumithrarachchi, S. Triambak, N. Warr, J. Wong, J. L. Wood, and S. W. Yates, *Phys. Rev. C* **101**, 044302 (2020).
- [39] A. Dewald, O. Möller, and P. Petkov, *Progress in Particle and Nuclear Physics* **67**, 786 (2012).
- [40] V. Karayonchev, J. Jolie, A. Blazhev, A. Dewald, A. Esmaylzadeh, C. Fransen, G. Häfner, L. Knafra, J. Litzinger, C. Müller-Gatermann, J.-M. Régis, K. Schomacker, A. Vogt, N. Warr, A. Leviatan, and N. Gavriyelov, *Phys. Rev. C* **102**, 064314 (2020).

- [41] T. Alexander and A. Bell, *Nuclear Instruments and Methods* **81**, 22 (1970).
- [42] A. Dewald, S. Harissopolos, and P. von Brentano, *Zeitschrift für Physik A Atomic Nuclei* **334**, 163 (1989).
- [43] J. Litzinger, A. Blazhev, A. Dewald, F. Didierjean, G. Duchêne, C. Fransen, R. Lozeva, K. Sieja, D. Verney, G. de Angelis, D. Bazzacco, B. Birkenbach, S. Bottoni, A. Bracco, T. Braunroth, B. Cederwall, L. Corradi, F. C. L. Crespi, P. Désesquelles, J. Eberth, E. Ellinger, E. Farnea, E. Fioretto, R. Gernhäuser, A. Goasduff, A. Görge, A. Gottardo, J. Grebosz, M. Hackstein, H. Hess, F. Ibrahim, J. Jolie, A. Jungclaus, K. Kolos, W. Korten, S. Leoni, S. Lunardi, A. Maj, R. Menegazzo, D. Mengoni, C. Michelagnoli, T. Mijatovic, B. Million, O. Möller, V. Modamio, G. Montagnoli, D. Montanari, A. I. Morales, D. R. Napoli, M. Niikura, G. Pollarolo, A. Pullia, B. Quintana, F. Recchia, P. Reiter, D. Rosso, E. Sahin, M. D. Salsac, F. Scarlassara, P.-A. Söderström, A. M. Stefanini, O. Stezowski, S. Szilner, C. Theisen, J. J. Valiente Dobón, V. Vandone, and A. Vogt, *Phys. Rev. C* **92**, 064322 (2015).
- [44] R. J. Estep, R. K. Sheline, D. J. Decman, E. A. Henry, L. G. Mann, R. A. Meyer, W. Stoeffl, L. E. Ussery, and J. Kantele, *Phys. Rev. C* **35**, 1485 (1987).
- [45] B. Saha, *Ph. D. thesis, Universität zu Köln* (2004).
- [46] G. Mamane, E. Cheifetz, E. Dafni, A. Zemel, and J. B. Wilhelmy, *Nuclear Physics A* **454**, 213 (1986).
- [47] E. Cheifetz, R. C. Jared, S. G. Thompson, and J. B. Wilhelmy, *Phys. Rev. Lett.* **25**, 38 (1970).
- [48] S. G. Rohoziński, J. Srebrny, and K. Horbaczewska, *Zeitschrift für Physik A Atoms and Nuclei* **268**, 401 (1974).
- [49] J. Dobaczewski, S. G. Rohoziński, and J. Srebrny, *Zeitschrift für Physik A Atoms and Nuclei* **282**, 203 (1977).
- [50] *γ -soft code*, <http://kody.slcrj.uw.edu.pl/index.php> (2020).
- [51] R. Casten, P. Von Brentano, K. Heyde, P. Van Isacker, and J. Jolie, *Nuclear Physics A* **439**, 289 (1985).
- [52] P. Lipas, P. Toivonen, and D. D. Warner, *Physics Letters B* **155**, 295 (1985).
- [53] S. Lalkovski and P. Van Isacker, *Phys. Rev. C* **79**, 044307 (2009).
- [54] S. Heinze, *Ph. D. thesis, Universität zu Köln* (2008).
- [55] R. F. Casten, *Journal of Physics G: Nuclear and Particle Physics* **42**, 034029 (2015).
- [56] E. A. McCutchan, D. Bonatsos, N. V. Zamfir, and R. F. Casten, *Phys. Rev. C* **76**, 024306 (2007).
- [57] A. E. L. Dieperink, O. Scholten, and F. Iachello, *Phys. Rev. Lett.* **44**, 1747 (1980).
- [58] J. N. Ginocchio and M. W. Kirson, *Phys. Rev. Lett.* **44**, 1744 (1980).
- [59] Böyükata, M., Ellinger, E., Fransen, C., and Jolie, J., *EPJ Web of Conferences* **66**, 02013 (2014).
- [60] *National Nuclear Data Center* (2020).
- [61] G. Lhersonneau, J. C. Wang, S. Hankonen, P. Dendooven, P. Jones, R. Julin, and J. Äystö, *Phys. Rev. C* **60**, 014315 (1999).
- [62] H. Toki and A. Faessler, *Zeitschrift für Physik A Atoms and Nuclei* **276**, 35 (1976).
- [63] E. A. Stefanova, S. Lalkovski, A. Korichi, T. Kutsarova, A. Lopez-Martens, F. R. Xu, H. L. Liu, S. Kisyov, A. Minkova, D. Bazzacco, M. Bergström, A. Görge, F. Hannachi, B. Herskind, H. Hübel, A. Jansen, T. L. Khoo, Z. Podolyák, and G. Schönwasser, *Phys. Rev. C* **86**, 044302 (2012).
- [64] S. Lalkovski and N. Minkov, *Journal of Physics G: Nuclear and Particle Physics* **31**, 427 (2005).
- [65] I. Deloncle, A. Bauchet, M. G. AU Porquet, M. Girod, S. Péru, J. P. Delaroche, A. Wilson, B. J. P. Gall, F. Hoellinger, N. Schulz, E. Gueorguieva, A. Minkova, T. Kutsarova, T. Venkova, J. Duprat, H. Sergolle, C. Gautherin, R. Lucas, A. Astier, N. Buforn, M. Meyer, S. Perriès, and N. Redon, *The European Physical Journal A* **8**, 177 (2000).